

FATIGUE STRENGTH OF A CHASSIS OF A SEMI-HEAVY TRUCK UNDER DYNAMIC LOADS DUE TO REAL ROAD ROUGHNESS

UDC 621.629

Summary

Evaluation of fatigue life of vehicles by using a real road test is very expensive; therefore, numerical methods such as Finite Element Method (FEM) are nowadays very popular for evaluating fatigue life. In this study, a method based on FEM is proposed for predicting fatigue strength of the chassis when designing and optimizing a semi-heavy truck. An experimental modal analysis has been applied for the validation of the finite element model which has been used in the proposed method. The natural frequencies and mode shapes of the chassis have been obtained from the finite element analysis and compared with the corresponding results of the experimental modal analysis. Also, a method for producing uneven roads in the time domain based on the International Reference Index (IRI) was introduced to simulate road roughness. In addition, different road types (with potholes and kerbs) and different load conditions (braking and cornering) have been considered throughout the simulation. In all of the mentioned conditions, stress time histories have been extracted and investigated. Finally, fatigue damage and strength of the chassis and welded connections have been estimated and described.

Key words: truck chassis, road profile, modal analysis test, finite element analysis, fatigue strength, breaking, cornering.

1. Introduction

Fatigue is an important factor which reduces the strength of material subjected to variable loads over time. It is accompanied by displacement of atomic layers and is a source of the spreading of microscopic cracks on the vehicle body. The spreading of these microscopic cracks causes fatigue on mechanical parts. Fracture due to fatigue occurs suddenly and it is dangerous, therefore, it is necessary to determine the endurance limit and fatigue life of vehicle parts. Fatigue damage on vehicle parts is related to the quality of roads on which vehicles are driven, as well as to the speed of the vehicle, the type of moving (straight, rolling, breaking, moving along uneven roads) and etc. Vehicle companies have programmes for fatigue testing of vehicle parts such as chassis in order to estimate fracture strength of the chassis during straight moving on roads of different qualities over a distance of

200,000 km (design life) [1]. Fatigue analysis has also been performed only on real roads [2]. Evaluation of fatigue strength by using a test on a real road is very expensive; also the use of results from the test and calculating the fatigue damage is complicated. Therefore, in order to reduce the specimen number (e.g. expensive prototypes) and to shorten the testing procedures (i.e. period of obtaining results), Beaumont and et al. presented an overview of accelerated life tests (AFT) in 2012 [3]. These methods do not involve high frequency load cycling, but are mainly based on stress magnification and fatigue damage equivalence. As a result, nowadays numerical methods, especially the FEM, are commonly applied for the evaluation of fatigue damage of the chassis. In recent years, for fatigue damage calculation, CAD-CAE has been used in the design and analysis of the structure and vehicle body by moving a model of the vehicle along simulated roads [4]. In 2012, Muhammad Nor and et al. [5] performed a stress analysis on a low loaded chassis by FEM using a 3-D model in CATIA. Further, Rahman and et al. [6] studied life prediction of a heavy duty truck. The analysis was done for a truck model by utilizing a commercial finite element package ABAQUS. The authors obtained the stress magnitude of the critical point as an initial to probable failure since fatigue failure started from the highest stress point. Moreover, some researchers have done the stress analysis of the chassis frame for design modification [7]. Among them, Koibuch [8] prepared software for predicting the fatigue strength of vehicle parts in 1998. Kawamura and et al. [9] used numerical methods to produce road roughness profiles and studied the fatigue life of vehicle parts by moving vehicles along these road profiles. Kawamura and et al. [9] and Davis and Thompson [10] also defined road roughness using Power Spectral Density (PSD), by which they calculated loads due to the road profile and applied them to the vehicle body to obtain the stress distribution. Also, Ramji and et al. [11] used ISO standards to classify road roughness based on the PSD method in 2001. A review of fatigue analyses of automobile frames was discussed in detail by Chetan and et al. [12] in 2012. Recently, in 2000, an experimental modal analysis was applied for the finite element model validation by Ewins [13], but by now there has been not any work to validate the finite element model of a truck by this method. Therefore, in this paper, after the exact finite element modelling of the chassis, the experimental modal analysis was applied for validating the finite element model. It should be mentioned that other parts are modelled approximately so as to consider their weights. Finally, the strength of the chassis is studied against road excitations with the application of different types of loads on the chassis because of braking and cornering. The flowchart of the method used in this study is shown in Fig. 1.

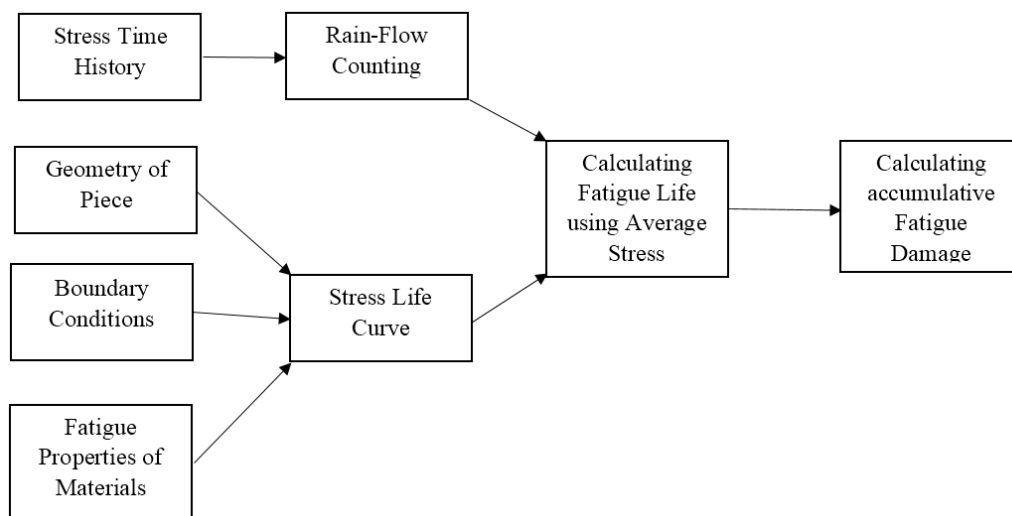


Fig. 1 Flowchart of the method

2. Modelling of truck, chassis and connections

2.1 Truck chassis and loads

The chassis of semi heavy trucks, similar to the chassis presented in Fig. 2, are usually of the ladder type and they make the whole structure of the truck together with the body and skin panels. This type of chassis is made of special U shape profiles which are joined by rivets, bolts or weld elements. The thickness of these profiles is about 4 to 5 mm, and they are made from low or moderate-carbon steels such as St-44-2 that exhibit low sensitivity to stress, high endurance and resistance to yielding, in addition to having high welding ability and cold state-formability. Generally, throughout the process of the truck chassis design, the safety factors of fatigue and endurance limit should be conservative. The considered chassis material is made of average carbon steel with a 290 MPa yield stress and 530 MPa ultimate tensile stresses [14, 15]. Also, the modulus of elasticity, density and the Poisson coefficient is 200 GPa, 7800 kg/m³ and 0.31, respectively.

All vehicles are subjected to both static and dynamic loads. Dynamic loads are caused by the moving of the vehicle on rough roads, while static loads are caused by the weight of the vehicle. Other loads result from braking, accelerating, and cornering of the vehicle. A simplified free-body diagram of the major loads which act on the vehicle is shown in Fig.3. Symmetric loads acting in the vertical direction predominantly cause bending of the chassis side members. Vertical loads arise from lateral loads acting parallel to the frame plane during cornering [16]. In addition, loads imposing on the plane of the frame cause bending of the side members and of the cross-members [1, 16].

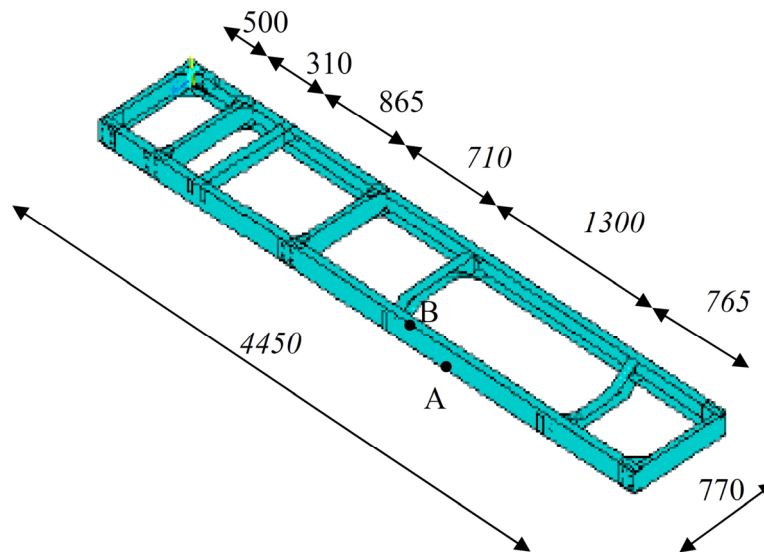


Fig. 2 Ladder chassis of the truck (Dimensions are in mm)

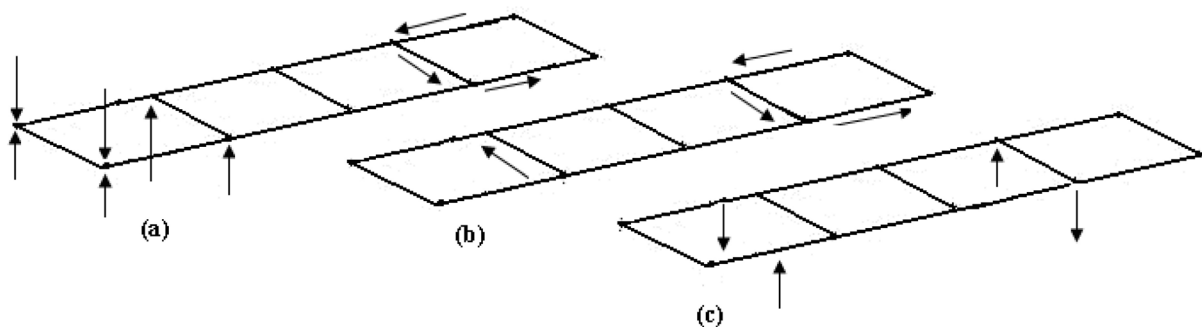


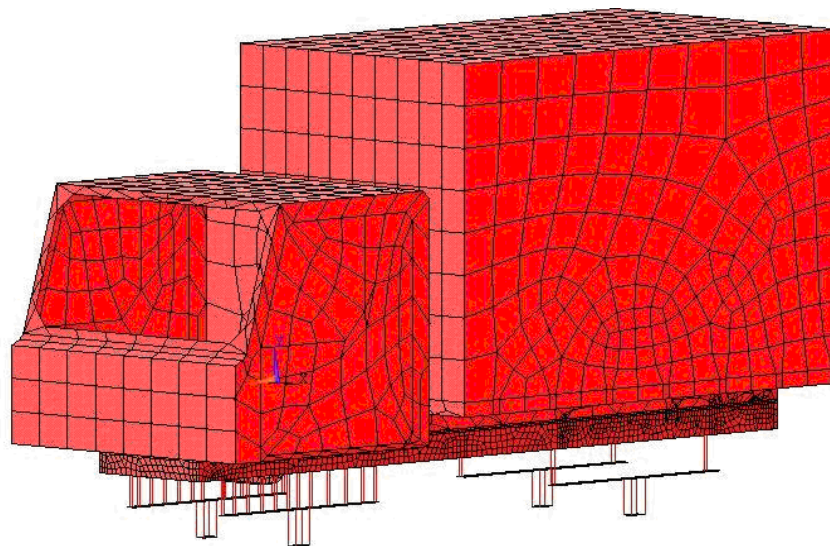
Fig. 3 Loads on the chassis
a) Torsion and bending loads during cornering, b) Transverse load and c) Torsion load

2.2 Finite element modelling

For the finite element modelling of the truck, first, a 3D model has been developed in the ANSYS software. For this purpose, shell 63 elements were used. The cabin and the truck were also included in this model. Mass and other mechanical properties of the model were applied based on accurate measurements of real parts. Since there are shock absorbers and springs between the truck and the chassis, these elements were also added to the model. The final 3D FE model is shown in Fig. 4.

The stiffness of the springs and their strength were defined and modelled by using combined 14 elements. Additionally, plates with a defined mass were placed between the springs to act as unsprung mass. The model, which was developed so that a dynamic analysis can be carried out, is shown in Fig.5. This model is a combination of sprung mass (M_s), unsprung mass (m_i), tire damping coefficient (C_t), suspension springs (K_i), and suspension dampers (C_i) [17, 18].

Table 1 shows the values of sprung and unsprung mass, stiffness and the damping coefficient of tires in suspension systems [14].



Truck Finite Element Model

Fig. 4 FE model of the truck

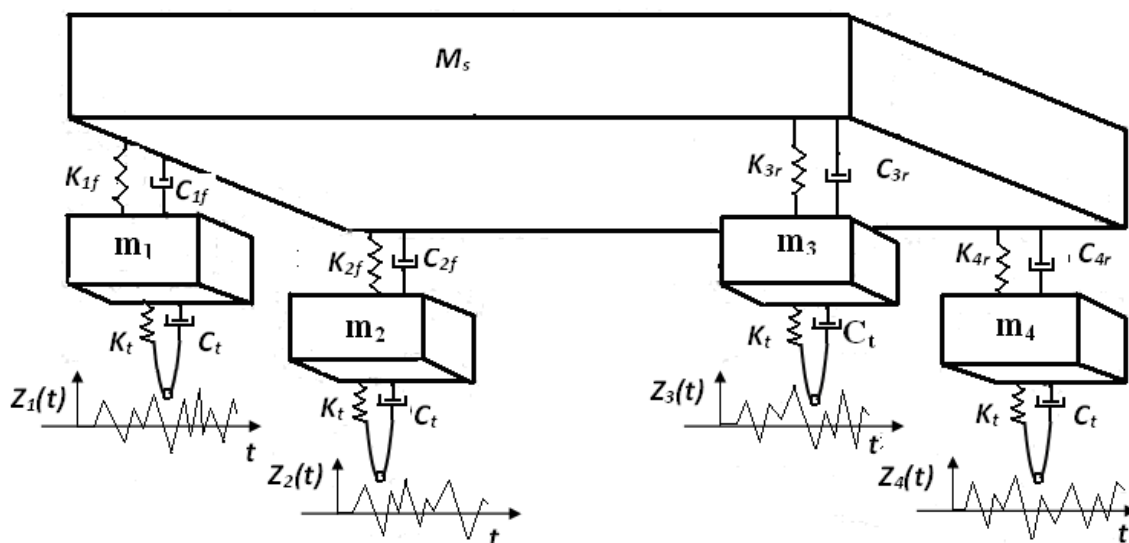


Fig. 5 Simulation model for applying dynamic loads

Table 1 Parameters of tires and suspension model

Case	Value	Unit
M_s , (sprung mass)	50	kN
m_1, m_2, m_3, m_4 (unsprung masses)	5	kN
K_t (tire stiffness)	177	kN/m
C_t (tire damping)	2860	Ns/m
K_{1f}, K_{2f} (front suspension spring)	85	kN /m
K_{3r}, K_{4r} (rear suspension spring)	250	kN /m
C_{1f}, C_{2f} (front suspension damper)	58	Ns/m
C_{3r}, C_{4r} (rear suspension damper)	68	Ns/m

2.3 Validation of the chassis model by experimental modal analysis

The experimental modal analysis to obtain the dynamic behaviour of a system has been extensively discussed in literature [19-21]. Stages of the experimental modal analysis of a system are firstly based on producing a prototype of a system and imposing actuating forces on this system; then the forces and the response of the system are measured. By extracting the Frequency Response Function (FRF), vibration parameters may be identified. The approach called the experimental modal analysis is different from the approach which uses the theoretical modal analysis. In the latter, governing equations should be constructed and by solving them, a modal model can be obtained and finally the response of the system may be calculated whereas in the experimental modal analysis, a real system is considered and modal parameters are estimated. This major difference reveals the advantage and accuracy of the method using the experimental modal analysis. The basics of the identification methods to analyse the experimental data which are gathered from the modal test analysis are explained here briefly.

A real structure is usually assumed to be a set of discontinuous and separate points with different degrees of freedom (DOFs). The governing equations of the behaviour of the system with N DOF with damping are [22]:

$$[M]\{\ddot{x}\} + [C]\{\dot{x}\} + [K]\{x\} = \{F(t)\} \quad (1)$$

in which $[M]$ is the mass matrix, $[C]$ is the viscous damping matrix, $[K]$ is the stiffness matrix and $\{x\}$ is the system response vector in a specific DOF. Also $\{F(t)\}$ is the external applied force vector. The Laplace transform of equation (1) yields:

$$[Ms^2 + Cs + K] X(s) = F(s) + (Ms + C) x(0) + M\dot{x}(0) \quad (2)$$

The modal model is fully described by a matrix of frequency response functions, $\mathbf{H}_{pq}(\omega)$, where its elements may be obtained by calculating the ratio of the response signal in the frequency domain at DOF p , $\mathbf{X}_p(\omega)$, to the input force signal in the frequency domain at DOF q , $\mathbf{F}_q(\omega)$, in the frequency domain [23]:

$$\mathbf{H}_{pq}(\omega) = \frac{\mathbf{X}_p(\omega)}{\mathbf{F}_q(\omega)} \quad (3)$$

Assuming the zero initial condition and knowing that the mode shape vectors are orthogonal with respect to the mass and stiffness matrixes, Eq. (3) may be written in a matrix form as follows:

$$\mathbf{X}(\omega) = \mathbf{H}(\omega) \cdot \mathbf{F}(\omega) \quad (4)$$

where

$$\mathbf{H}(\omega) = [\mathbf{K} - \omega^2 \mathbf{M} + i\omega \mathbf{C}]^{-1}$$

or:

$$\mathbf{H}(\omega) = [\Phi] \begin{bmatrix} 0 & & \\ & \frac{1}{\omega_r^2 - \omega^2 + i\eta_r \omega_r^2} & \\ & & 0 \end{bmatrix} [\Phi]^T$$

where $[\Phi]$ is the mass-normalized form of the mode shape vectors. The relationship between the natural frequencies, mode shapes and the elements of $\mathbf{H}(\omega)$ matrix can be obtained [24, 25] as follows:

$$\mathbf{H}_{pq}(\omega) = \sum_{r=1}^N \frac{\varphi_{ir} \varphi_{jr}}{\omega_r^2 - \omega^2 + i\eta_r \omega_r^2} \quad (5)$$

where φ_{ij} are the members of the mass-normalized mode shape matrix.

In the first step of the experimental modal analysis, the elements of at least one full line or one full column of the FRF matrix should be measured. In the next stage, for calculating the modal parameters, the maximum points in every diagram, which refers to the natural frequency of the system, are selected and the natural frequency and damping coefficient ratio are calculated by using the frequency response at these points. The ratio between the amplitudes of different frequency response diagrams in a certain natural frequency shows the shape and mode of vibration at this frequency.

Now, to validate the finite element model of the chassis, a modal analysis has been carried out in the free-free condition (Fig. 6). For this purpose, the chassis was suspended along its symmetry axes from the frame by using a hook attached to the chassis. A hammer test was used to provide required exciting forces on the structure. In this test, a hammer (Type 8202, B &K Inc., Denmark) and four accelerometers (type 4504, B & K Inc., Denmark with a sensitivity of 0.94 *pc/N*) were used. The mass of the hammer and the accelerometers is 21 and 14 grams, respectively. The excitation force has been applied to seven different points while the four accelerometers' positions were fixed (roving hammer method). Considering that the direction of the forces is along the Z-axis (see Fig. 5), the frequency response functions of the system were extracted from the mentioned points. The results were analysed and presented as FRF curves for different points of the chassis. As an example, one of the extracted FRFs is shown in Fig. 7. The measured frequency data range from 0 to 100 Hertz. Throughout the mentioned domain, twelve natural frequencies were estimated for the chassis, which are shown in Table 2. Also, for each natural frequency, a corresponding mode shape was identified. Fig. 8 shows the two typical mode shapes.

The difference/error between the frequencies which have been obtained by using the FEM analysis and the frequencies from the modal analysis is between 5 and 10 per cent (see Table 2). The errors can be attributed to the simplifying assumptions, limitations in finite element modelling, and other parameters related to the experiment itself and the accuracy of the measurements. The simplified modelling of the chassis, the assumption of the unitized body and neglecting the contact areas in joints can also be sources of this error. Common sources of error, including data acquisition, leakage, windowing, filtering and other computational errors exist and

may affect the results [13]. Other experiment limitations such as variation of the applied transient force in the hammer test also exist [26]. The results, in spite of the 5 to 10 per cent error level, and six zero first modes prove that the numerical FEM based solution is accurate and reliable.



Fig. 6 Experimental modal test (suspended by a hook)

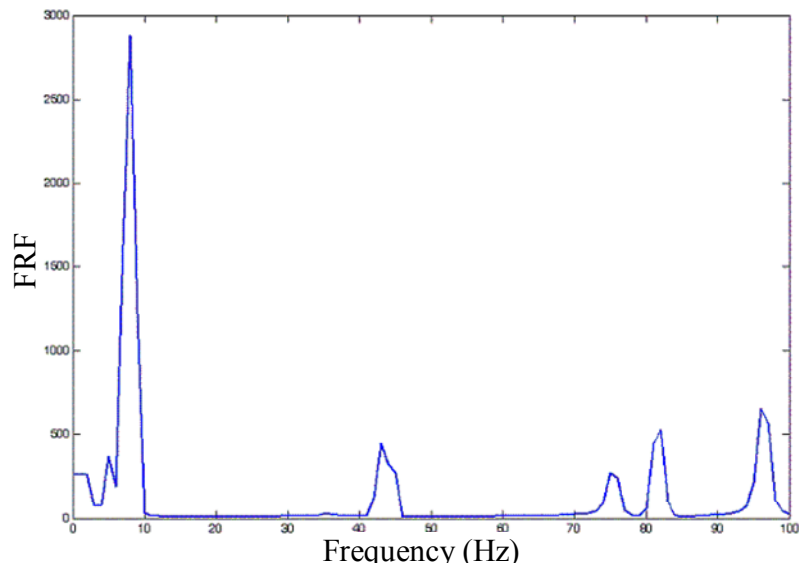


Fig. 7 Typical frequency response function (FRF) of modal analysis

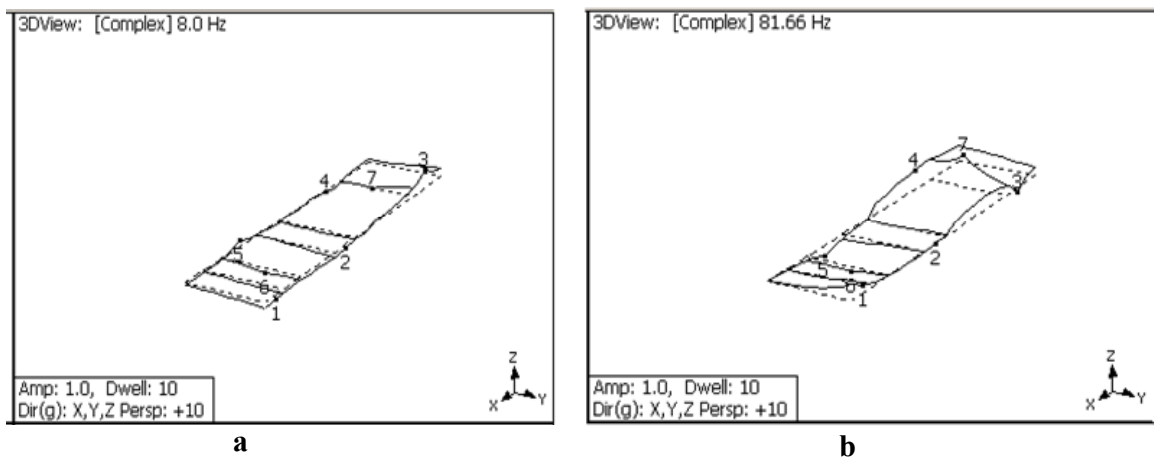


Fig. 8 Typical mode shapes obtained from modal analysis
a) Chassis mode shape corresponding to natural frequency of 8 Hz
b) Chassis mode shape corresponding to natural frequency of 81.66 Hz

Table 2 Comparison of the natural frequencies of specified mode shapes between modal analysis tests and FEM

Case	FEM /Hz	Experimental (Modal Analysis Test)	Experimental (Modal Analysis Test) /Hz	Error /%
1	0	-	Rigid	-
2	0	-	Rigid	-
3	0	-	Rigid	-
4	0	-	Rigid	-
5	0	-	Rigid	-
6	0	-	Rigid	-
7	8.66	8	1 st Bending Mode	5
8	29.6	26.71	2 nd Bending Mode	10
9	37.9	34.54	3 rd Bending Mode	10
10	52.09	43.21	Combined undefined mode shape	-

2.4 Simulation of boundary condition

The boundary conditions are applied to the position of the connection between the spring elements and the chassis. Also, the unsprung mass of the truck has been distributed on the plates, between the spring elements. In addition, the displacement of the truck in the directions of the axial and the lateral axis at the mentioned boundaries should be constrained because the spring of the truck is linear. Also, because the truck does not rotate around the perpendicular axis of its body (yaw), the truck rotation, the motion of the longitudinal and lateral directions should be constrained. Now, by considering the mentioned boundaries, road roughness, considered as random load, can be applied to the truck as it is seen in Fig.5.

2.5 Simulation of road roughness

When the vehicle moves along the road, the displacement induced by the road is applied to the chassis over the front wheels and it is also applied to the rear wheels with a time delay. The time delay is equal to the distance between the front and rear axis, divided by the vehicle speed. Because of the chassis mass the mass on the front wheels is as follows:

$$m_{of1} = \frac{1}{2} \frac{b}{c+b} M_o \tag{6}$$

where M_o is the chassis mass, b and c are the distances of gravity centre from the front and the rear axis, respectively.

Now, by considering Fig. 5, the differential equations, related to one of the front wheels are as follows:

$$m_{of1} \ddot{x}_2 + c_d(\dot{x}_2 - \dot{x}_1) + k_d(x_2 - x_1) = 0 \tag{7}$$

$$m_1 \ddot{x}_1 + c_t(\dot{x}_1 - \dot{z}_d) + k_{pd}(x_1 - z_d) = 0 \tag{8}$$

In the above formula, m_1 denotes the unsprung mass. Also c_t , c_d , k_{pd} and k_d are the tire damping coefficient, the suspension system damping coefficient, the tire stiffness and the leaf spring stiffness, respectively. In addition, x_1 and x_2 are displacements, associated with m_1 and m_{of1} , respectively. Finally, z_d is the displacement due to road roughness. Using the same

equations for other wheels of the truck, it is possible to derive the displacement of the truck chassis by numerical methods. Hence, road roughness may be simulated by a stationary stochastic process with the Gaussian probability distribution function [10].

In the stochastic process, the correlation function is very important and is defined as follows:

$$R(\tau) = \lim_{T \rightarrow \infty} \frac{1}{T} \int_0^T Z_d(t)Z_d(t - \tau)dt \quad (9)$$

In the above equation, $Z_d(t)$ is the road roughness function. If the stochastic process and the mean of the road roughness are normal and zero, respectively, then the standard deviation (STD) of the road can be derived. In this condition, $R(0)$ will be the square of the STD [10].

Now, road roughness in the time domain can be produced by applying Eq. (9). Also, STDs of different roads are available in Table 3 [9]. The classification of surface roughness by ISO and corresponding PSD can be found in Fig. 9.

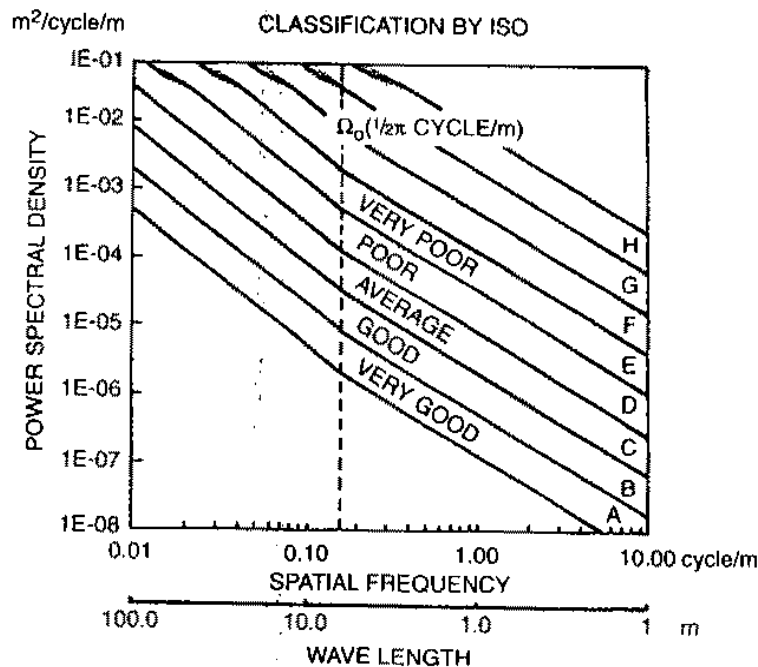


Fig. 9 Classification of surface roughness by ISO

2.6 Effective loads for fatigue of chassis

In practical applications, the truck components are under random loads. Therefore, the stress variation due to random loads should be analysed for the evaluation of the chassis strength. The information bank, applied for the structural fatigue analysis, has several components so that each component makes a definite percentage of the whole information. The mentioned percentage has been defined based on individual standard. Generally, the results of the following four states, related to the information bank, should be considered:

1. Moving on uneven roads
2. Driving over potholes and kerbs
3. Braking with maximum retardation
4. Cornering with maximum lateral acceleration

The first state is very important because it causes fatigue of the vehicle structure, which is caused by bending and torsion loads. Thus, the simulation of the two first states will be

described; then, the time history of stress will be extracted by using the dynamic analysis. In other states, the statistical analysis in critical condition will be carried out for the evaluation of the derived stresses.

2.7 Simulation of uneven real roads and extracting stress time histories

The life of the vehicle structure is travelling 200,000 km on different roads. Also, velocity of the road test is one of the important parameters that are illustrated in Fig. 9 when the IRI criteria are considered. IRI is defined as the International Reference Index summarizing the road profile by a mathematical model representing the response of a traversing vehicle, and the reference average rectified slope of the axle-body displacement of a quarter-car” [8]. The standard deviation of some roads and their IRIs are in Table 3. Also, simulations of three different road roughnesses are presented in Fig. 10. With respect to the application of trucks, the amount of the truck travel on different roads has been determined based on experience (see Table 3). For example, 20% of the total vehicle moving (200,000 km) is on rough roads and the remaining moving is on roads of classes C, D and E. The traversing time can be calculated with the distance and constant speed of traversing, and then it is possible to simulate road roughness. Transient response with the direct method as a general method has been used for the dynamic response analysis and extracting the stress in different cycles. Thus, by identifying critical elements in accordance to the stress level, the maximum stress can be used for calculating the accumulative fatigue damage. Fig.11 shows stress levels (Von-Mises), corresponding to the two critical elements on a rough road.

Table3 STD, PSD and IRI of road roughness

Statistical Parameters	Road Type				
	Rough roads	Very poor roads	Average roads	Poor roads	Expressway
STD	17.8	3.3	3.4	3.2	0 (1E-8).7
PSD	E – F	C – E	C - D	C - D	A – B (1E-8)
IRI	15	7	2.5	4.3	1.5

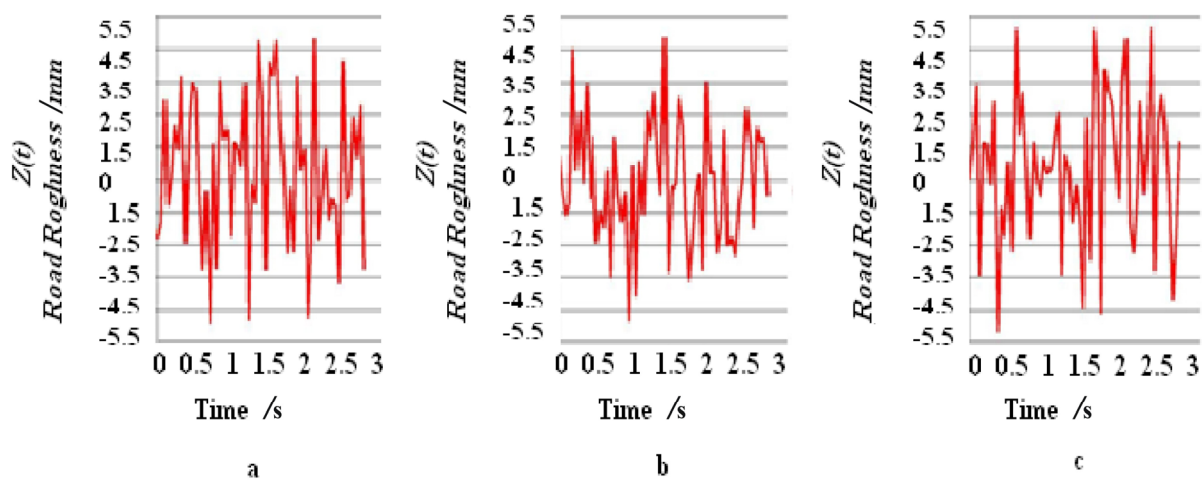


Fig. 10 Simulation of three different road roughnesses
a) Average roads; b) Very poor roads; c) Rough roads

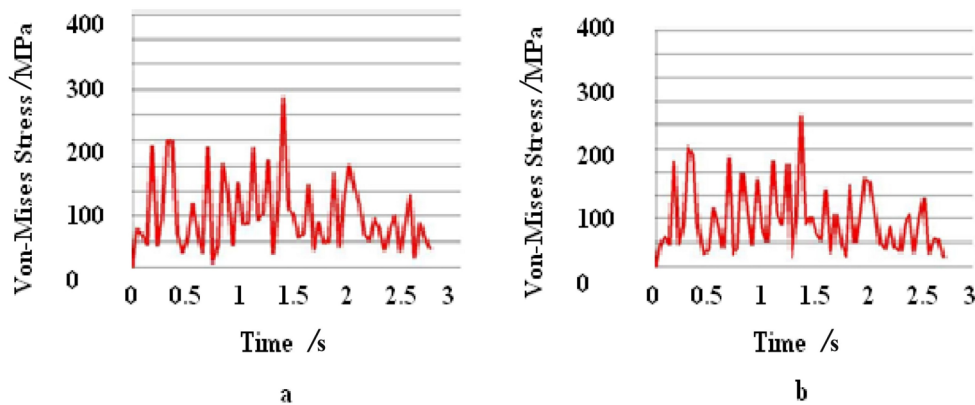


Fig. 11 Critical element of the stress level (Von-Mises) on rough road
a) Element No. 37037; b) Element No. 36692

2.8 Simulation of roads with potholes and kerbs

Potholes and kerbs of the road may be considered as sudden and transient inputs. Dimensions of potholes and kerbs are effective parameters in estimating the vehicle damage. The equation which specifies potholes of the road may be written as follows:

$$Z(t) = \begin{cases} -\frac{t}{2} & t < 0.1 \\ -y & 0.1 < t < 0.4 \\ \frac{-0.1 + (t - 0.4)}{2} & 0.4 < t < 0.5 \end{cases} \quad (10)$$

where y is the depth of a puddle and t denotes time. If $t - t_{\text{delay}}$ substitutes t in Eq. (10), the corresponding displacement equation for rear wheels may be available. Also, t_{delay} is the delay time of the front and the rear wheels, which is dependent on the speed and the distance of the mentioned wheels and it can be derived as follows:

$$t_{\text{delay}} = \frac{L}{V} \quad (11)$$

where, L and V are the wheel distance and speed, respectively. If Eq. (10) is multiplied by -1 , the equation will be corresponding to kerbs of the road. It should be mentioned that the speed is a very important parameter which can be a function of time and is dependent on the road type and traffic conditions. This speed is illustrated in Fig. 9 as a function of the road type and its IRI criteria [28].

3. Results and discussions

3.1 Stresses during moving on roads with potholes and kerbs

Different cases of driving over potholes and kerbs on roads have been considered and studied. The type of the road selected in this study is a very poor road, where the IRI of the road is 7, see Fig. 9. So, the speed of the truck is considered to be 80 km/h and y in Eq. (10) is selected as $y = 0.05$ m (Newland, D. E., 1984). Also, considering the distance between the front and the rear wheel (2.6 m), t_{delay} is equal to 0.12 s. The truck chassis is under bending and torsion loads while driving over potholes and kerbs in different cases. Some of the cases are the front wheels driving over kerbs simultaneously or separately. Analysing the Von-

Mises stresses derived for different cases, it may be found that the critical case occurs when one pair of a front wheel and a rear wheel on the opposite side drive over kerbs. Also, another critical case is when one of the wheels drives over kerbs. Figs. 12 and 13 illustrate corresponding equivalent stresses, extracted for the mentioned two cases. As it is obvious from these figures, the critical stresses are not greater than the fatigue endurance limit, but if the height of the kerbstone or depth of the potholes are more than 25 and 20 cm, respectively, this causes some stresses which are greater than the fatigue endurance limit, as illustrated in Figs. 14 and 15.

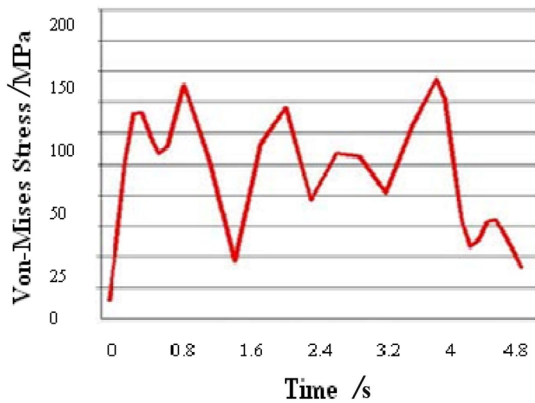


Fig. 12 Equivalent stresses (Von-Mises) due to driving over kerbs (kerbstone height=0.05 m)

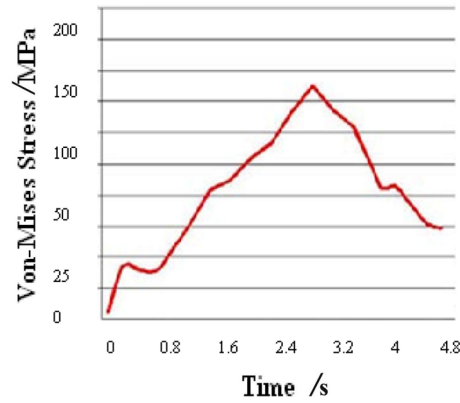


Fig. 13 Equivalent stresses (Von-Mises) due to driving over potholes (pothole depth=0.05 m)

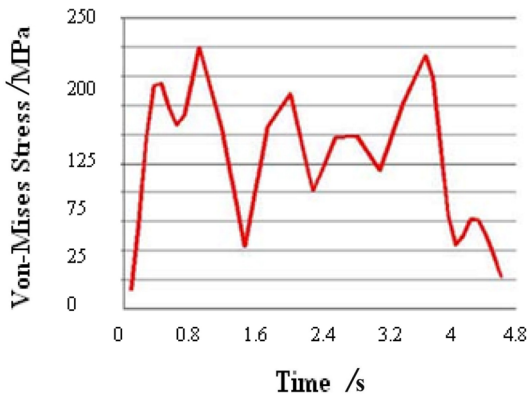


Fig. 14 Equivalent stresses (Von-Mises) due to driving over kerbs (kerbstone height=0.25 m)

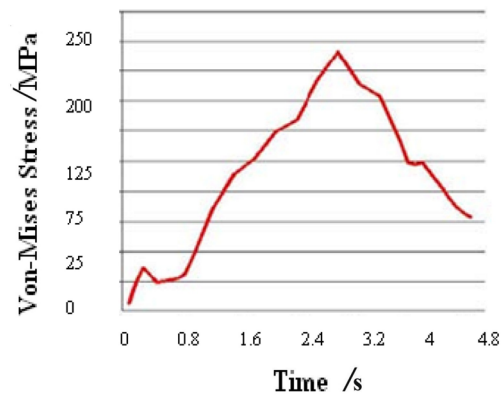


Fig. 15 Equivalent stresses (Von-Mises) due to driving over potholes (pothole depth=0.2 m)

3.2 Stresses during braking with maximum retardation

Maximum braking force is limited to the slip friction force between the road and the tire when all of the tires are locked. The maximum retardation of the trucks is considered as 7 m/sec^2 where the longitudinal forces are maximum. For simulating this case, the whole of the truck was accelerated at -7 m/sec^2 in its longitudinal direction while the model wheels were locked. The variations of the stresses are shown in Fig. 16. As it is obvious, the maximum stress is 75.3 MPa. By defining the ratio of the minimum to the maximum stress, as follows:

$$R = \frac{\sigma_{\min}}{\sigma_{\max}} \tag{12}$$

it was found that $R = 0$ in the mentioned case of the truck. Also, the variation of the stresses is less than the endurance stress (199 MPa), therefore, the chassis has enough strength against the applied forces. Additionally, Fig. 17 illustrates the displacement of the model during braking.

3.3 Stresses during cornering

In this case, the boundary condition of the model is similar to the previous case. In addition, the longitudinal force is increased from the inner to the outer tires during cornering. The maximum longitudinal acceleration of the vehicle is corresponding to the rollover instant where the acceleration of the truck is between 0.6 and 0.8 of the gravity acceleration. Considering the acceleration being equal to 0.7g in the transverse axial direction of the truck, the stresses can be extracted. Fig. 18 shows the truck behaviour during cornering. Also, taking Fig. 19 into consideration, the maximum stress is 93.3 MPa, which is lower than the fatigue endurance limit of the chassis. Thus, the chassis has enough strength in this case.

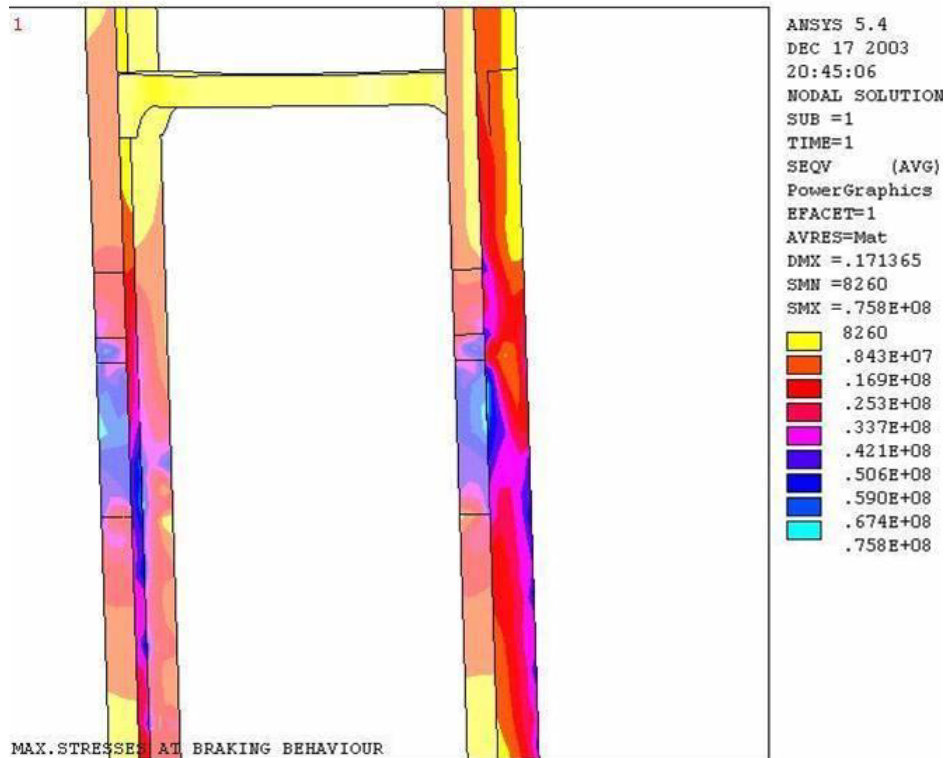


Fig. 16 Stress distribution during braking with maximum retardation

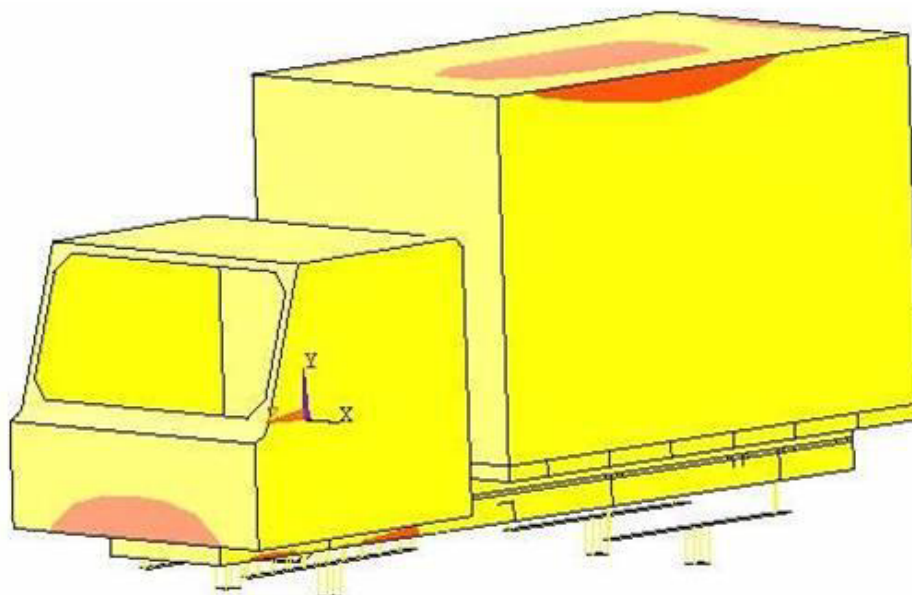


Fig. 17 Displacement behaviour of the model after braking with maximum retardation

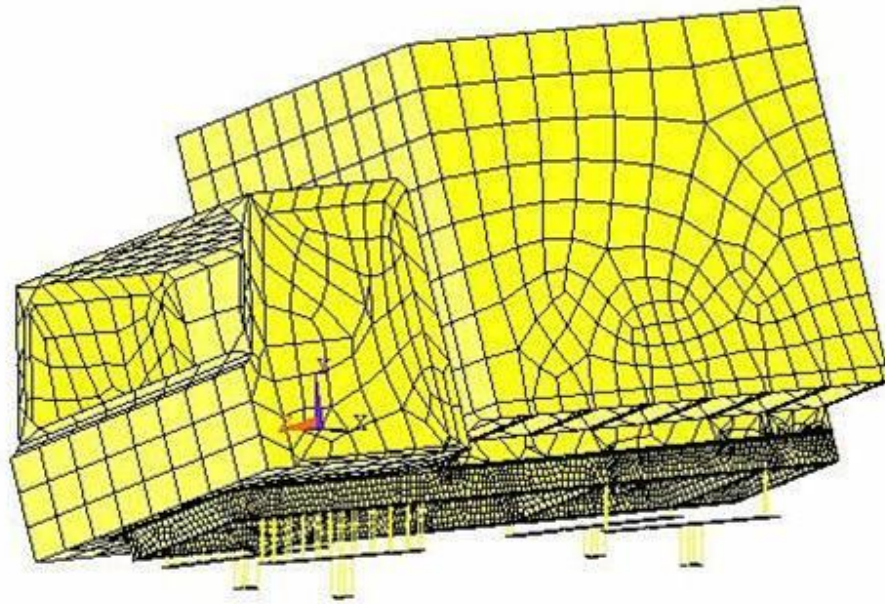


Fig. 18 Behaviour of the model during cornering with maximum lateral acceleration

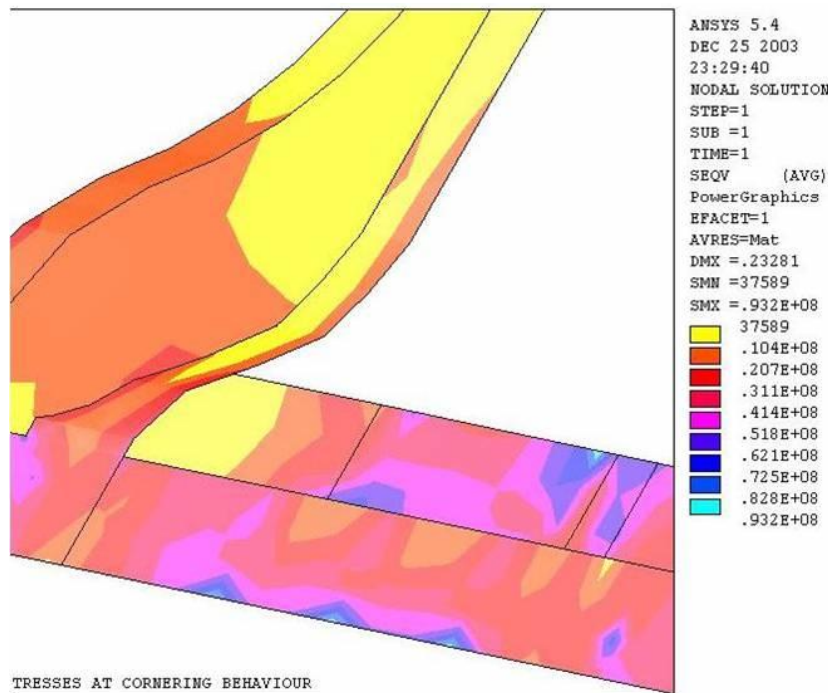


Fig. 19 Stress distribution during cornering with maximum lateral acceleration

3.4 Calculation of accumulative fatigue damage of the vehicle chassis

Considering that the chassis is subjected to random loads, Miner's rule is suitable for estimating the fatigue life as follows [30]:

$$\frac{n_1}{N_1} + \frac{n_2}{N_2} + \dots + \frac{n_i}{N_i} = C \quad (13)$$

where n_i is the number of the applied load cycle and N_i is the corresponding fatigue life at the constant stress level σ_i obtained from the σ - N curve. Also, C is determined based on experience which is usually between 0.7 and 2.2 [31]. Some researchers propose that $C = 1$.

As it was shown in the previous section, the critical stresses of the chassis, when truck is braking or cornering, are below the fatigue endurance limit, so these stresses do not affect the life of the chassis if Miner’s theory is considered, and the chassis life is infinite. In addition, it was shown that when the truck drives over potholes and kerbs of usual depth and height, low stresses will occur which do not have any effect on the chassis life, but if the depth and height of potholes and kerbs is more than 25 and 20 cm, respectively, the chassis will be damaged. In Table 4, the cycle numbers in which damage will occur, are available for different inputs based on Miner’s theory. Also, damage is calculated based on the rain-flow counting by using stress time histories.

By simulating a real road in Section 2-6, the fatigue cycle number was extracted by the software and the chassis life was calculated by the rain-flow counting method and the results are given in Table 5. The results show that when the truck moves on roads with STD and IRI of 17.8 and 15, respectively, the chassis will be damaged (See Table 5). Also, with an increase in travelling speed and distance, damage will be increased.

Table 4 Fatigue damage on critical elements based on Miner’s rule when truck moves on three different roads (design life is 200000 km).

Road type	Travelled Distance /km	Travelled velocity /km/h	IRI of each road	Element # 36692 (point “A” in Fig. 2)		Element #37037 (point “B” in Fig. 2)	
				Maximum stress /MPa	Accumulative fatigue damage, c	Maximum stress /MPa	Accumulative fatigue damage, c
Damaged road	40000	40	15	251	0.965	260	1.204
Road with potholes	60000	70	7	190	0.21	192	0.33
Very poor roads	100000	90	4.3	175	0.072	175	0.077
Total	200000				1.25	-	1.61

Table 5 Fatigue damage and extracted stresses in truck chassis for different kerbs and potholes

Condition type	Roughness type	Critical element number of welds	Critical element number when moving from roughness	Maximum stress in elements of welds /MPa	Maximum stress due to moving from roughness /MPa	Repetition number of moving from the rough road, C = 1
1	Road with kerbs with the height of 0.05 m	38523 (near point “B”)	36692 (near point “A”)	53	153	Unlimited life
	Road with kerbs with the height of 0.25 m	38523 (near point “B”)	36692 (near point “A”)	98	224	50000
2	Pothole with a depth of 0.05 m	36045 (near point “A”)	37037 (between point “A” and “B”)	61	113	Unlimited life
	Pothole with a depth of 0.02 m	36045 (near point “A”)	37037 (between point “A” and “B”)	101	213	6692

3.5 Investigation of fatigue strength of welded connections

Yoshitake and et al. [15] show that the ratio of the fatigue strength of welded plates to the fatigue strength of non-welded plates of the same material decreases with an increase in the tensional strength of plates. Also, when the stress intensity of the connections increases to 2.5, the fatigue stress intensity increases to 1.3. In addition, when considering residual stresses caused by the welding process, it was found that the fatigue strength of welded plates with tensional strength of 440 MPa (corresponding to the Azarakhsh truck) and 590 MPa can be

estimated by considering the fatigue stress factor of 1.3. Thus, based on Miner's rule and the study by Yoshitake and et al. [15] the welding connections of the chassis have enough strength.

4. Conclusion

Evaluation of the fatigue life of the chassis using a real test on roads is very expensive; therefore, numerical methods such as FEM are nowadays applied for the evaluation of fatigue life. Additionally, the experimental modal analysis is known as a useful method for validating the finite element model of the mechanical systems. Thus, in this study, using the experimental modal analysis for the validation of finite element model, a method has been proposed for predicting the fatigue strength of the chassis. Also, a method for producing uneven roads in the time domain has been introduced. The experimental modal analysis results prove that the numerical FEM based solution is accurate and reliable. In addition, by considering stresses during driving over potholes and kerbs, it has been shown that the critical stresses are not greater than the fatigue endurance limit, but if the height of the kerbstone or depth of the potholes are greater than 25 and 20 cm, respectively, this causes some stresses to be greater than the fatigue endurance limit. Also, it has been found that the critical case occurs when one pair of a front wheel and a rear wheel on the opposite side are driving over kerbs. Additionally, during braking and cornering, the estimated stresses are lower than the endurance limit; therefore, the chassis has enough strength. It has been found that by simulating a real road, the chassis will be damaged when STD and IRI are 17.8 and 15, respectively. Also, when the travelling speed and distance increase, the damage increases too. Finally, it has been concluded that the welded connection stresses do not exceed 104 MPa. Thus, based on Miner's rule, the welding connections of the chassis are strong enough.

Acknowledgement

We thank all members of the Vibration and Modal Analysis Lab at the University of Tabriz for their kind cooperation on carrying out the modal tests. Authors also appreciate the kind support and help of the Light Truck Manufacturing of Tractor Sazi Co. Tabriz, Iran.

REFERENCES

- [1] K.Kobayashi, K.Yamagushi, and T.Ikejiri. "On Fatigue Testing of Passenger Car Body Construction". *SAE 710281* (1971).
- [2] K.V.Smith and R.F.Stornant. "Cumulative Damage Approach to Durability Route Design". *SAE 791033* (1979).
- [3] P.Beaumont, F.Guérin, P.Lantieri, L.M.Facchinetti and M.G.Borret. "Accelerated Fatigue Test For Automotive Chassis Parts Design: An Overview". Reliability and Maintainability Symposium. (RAMS), Proceedings-Annual, IEEE (2012).
- [4] J. H.Canova. "Vehicle Design Evaluation Using the Digital Proving Ground". *SAE 2000-01-0126* (2000).
- [5] M.A.Muhammad Nor, H.Rashid, W.F.M.W. Mahyuddin, M.A.M. Azlan and J.Mahmud. "Stress Analysis of a Low Loader Chassis". *Procedia Engineering*, Vol. 41, pp. 995-1001 (2012).
- [6] A.R.Rahman, N.M.Tamin and O.Kurdi. "Stress analysis of heavy duty truck chassis as a preliminary data for its fatigue life prediction using FEM". *Journal Mekanikal*, No. 26, pp. 76 -85 (2008).
- [7] P.V.Vijaykumar. "Structural Analysis of Automotive Chassis Frame and Design Modification for Weight Reduction". *International Journal of Engineering Research & Technology*, Vol. 1(3) (2012).
- [8] k.Koibuch. "Fatigue Life Prediction and its Software". Speech collection for JSAE symposium, New Proposals for Future Fatigue Endurance from the Basis of Road Profile Measurements, SAE Inc. (1998).
- [9] A.Kawamura, S.Nakojima, M.Yokota, T.Nakatsuji and K.Saito. "Prediction for truck endurance from the basis of road profile measurements". *SAE 107*, pp. 529-536 (1998).
- [10] B.R.Davis and A.G.Thompson. "Power spectral density of road profiles". *Vehicle System Dynamics*, Vol. 35, pp. 409-415 (2001).

- [11] K.Ramji, A.Gupta, V.Saran, V.Geal and V.Kumar. "Roadroughness measurements using PSD approach". *Journal of the Institution of Engineers*, Vol. 85, pp. 193-201 (2004).
- [12] J.S.Chetan, P.C.Khushbu and P.Fajalhusen. "A Review of the Fatigue Analysis of an Automobile Frames". *International Journal of Advanced Computer Research*, Vol. 2 (4) (2012).
- [13] D.J. Ewins. "Model Testing: Theory, Practice and Application". 2nd Edition, Research Studies Press Ltd., Bladock, Hertfordshire, England, pp: 163-284 (2000).
- [14] M.Shakori. "Experimental tests on the suspension system of the vehicle". Internal report, Light truck manufacturing Co., ITC Co., 1385-6, Tabriz, Iran (2004).
- [15] A.Yoshitake, M. Kinoshita, K. Osawa, H. Nakagawa and M. Kabasawa."Fatigue properties of fillet welded lap joints of high strength steel sheets for automobiles". *SAE*, Vol. 103, pp. 142-147 (1994).
- [16] H. J.Beermann. "The Analysis of Commercial Vehicle Structure". Mechanical Engineering Publication Ltd., London, 1st Edition, pp: 30-45 (1989).
- [17] A.Marco and J.Rogeria. "Dynamical simulation and structural analysis of light vehicles chassis". *SAE* 952280, pp. 1-8 (1995).
- [18] J. Y.Wong. "*Theory of Ground Vehicles*". 3rd Edn, John Wiley and Sons Inc., New York, USA., ISBN-10-0471354619, pp. 443-453, 528 (2001).
- [19] L.Hermans and H.Van Der Auweraer. "Modal testing and analysis of structures under operational conditions:Industrial applications". *Mechanical Systems and Signal Processing*, Vol. 13, pp. 193-216 (1999).
- [20] J. P. Yang and S. X.Chen. "Vibration predictions and verifications of disk drive spindle system with ball bearings". *J. Comput. Struct*, Vol.80, pp. 1409-1418 (2002).
- [21] P.Coucke, De J.Ketelaere and De. Baerdemaeker. "Experimental analysis of the dynamic and Mechanical behaviour of a chicken egg". *Journal of Sound and Vibration*, Vol. 266, pp. 711-721 (2003).
- [22] L.Meirovitch. "*Analytical Methods in Vibrations*". 1st Edition, Macmillan Publishing Co. Inc., NY, USA, ISBN: 0023801409, pp. 135-154 (1967).
- [23] A.Dimaragonas and S. Haddad. "*Vibrations for Engineers*", 2nd Edition. Prentice-Hall International Inc., ISBN-10: 0139526803, pp. 422-712 (1992).
- [24] J.H.Ginsberg. "*Mechanical and Structural Vibrations: Theory and Application*". New York., 1st Edition. John Wiley and Sons, Inc., New York, ISBN 0-471-37084-3 (2001).
- [25] N.M.M.Maia and J.M.M.Silva. "*Theoretical and Experimental Modal Analysis*". Facsimile Edition, John Wiley and Sons Inc., New York, ISBN: 0471970670, pp. 43-79 (1997).
- [26] N.Larbi and J.Lardies. "Experimental modal analysis of a structure excited by a random force". *Mechanical Systems and Signal Processing*, Vol. 14, pp. 181-192 (2000).
- [27] B.R.Davis and A.G.Thompson. "Power spectral density of road profiles". *Vehicle System Dynamics*, Vol. 35, pp. 409-415 (2001).
- [28] M.W.Sayers. "*On the Calculation of International Roughness Index from Longitudinal Road Profile*". Transportation Research Record, Issue No. 1501, Transportation Research Board, Washington, DC, USA, ISBN: 0309061695, pp: 1-12 (1995).
- [29] D. E.Newland. "*An introduction to random vibrations and spectral analysis*". 2nd ed. Longman Inc., New York, ISBN: 0-582-30530-b (1984).
- [30] J.A.Bannantine and J.J. Comer, J. L. "Handrock *Fundamentals of Metal Fatigue Analysis*". Prentice Hall (1990).
- [31] J. E.Shigley and C. R.Mischke. "*Mechanical Engineering Design*". Mc. Graw-Hill (1989).

Submitted: 11.8.2013

Accepted: 10.12.2014

Professor Mohammad Zehsaz
Professor Morteza Homayoun Sadeghi
Assist. Prof. Mir Mohammad Etefagh
Assist. Prof. Reza Hassannejad
Department of Mechanical
Engineering, University of Tabriz,
Tabriz, Iran
zehsaz@tabrizu.ac.ir